Appl. Numer. Math. 218 (2025) 128–147

Contents lists available at ScienceDirect

Applied Numerical Mathematics

journal homepage: www.elsevier.com/locate/apnum

Research Paper

Semi-implicit fully exactly well-balanced schemes for the two-layer shallow water system

C. Caballero-Cárdenas [a,*], M.J. Castro [b], C. Chalons [c], T. Morales de Luna [b], M.L. Muñoz-Ruiz [b]

[a] Facultad de Negocios y Tecnología, Universidad Alfonso X el Sabio – Mare Nostrum, Camino de la Térmica, 90, 29004 Málaga, Spain,
[b] Departamento de Análisis Matemático, Estadística e I.O. y Matemática Aplicada, Facultad de Ciencias, Universidad de Málaga, 29010 Málaga, Spain
[c] Laboratoire de Mathématiques de Versailles, Université Versailles Saint-Quentin-en-Yvelines, 45 Avenue des États-Unis, 78035 Versailles cedex, France

ARTICLE INFO

MSC:
76M12
35L60
65M08

Keywords:
Fully exactly well-balanced schemes
Relaxation schemes
Semi-implicit schemes
Two-layer shallow water system

ABSTRACT

This work addresses the design of semi-implicit numerical schemes that are fully exactly well-balanced for the two-layer shallow water system, meaning that they are capable of preserving every possible steady state, and not only the lake-at-rest ones. The proposed approach exhibits better performance compared to standard explicit methods in low-Froude number regimes, where wave propagation speeds significantly exceed flow velocities, thereby reducing the computational cost associated with long-time simulations. The methodology relies on a combination of splitting strategies and relaxation techniques to construct first- and second-order semi-implicit schemes that satisfy the fully exactly well-balanced property.

1. Introduction

Our main interest is the design of numerical schemes with good properties for the approximation of systems of conservation laws in which, in addition to a flux and a source term, non-conservative products may appear. In particular, we focus our attention on the two-layer shallow water system.

The two-layer shallow water system expresses the evolution in space $x \in \mathbb{R}$ and time $t \geq 0$ of a fluid composed of two layers of immiscible liquids with densities $\rho_1 < \rho_2$. This model is given by

$$\begin{cases} \partial_t h_1 + \partial_x (h_1 u_1) = 0, \\ \partial_t (h_1 u_1) + \partial_x \left(h_1 u_1^2 + g \dfrac{h_1^2}{2} \right) + g h_1 \partial_x h_2 = -g h_1 \partial_x z, \\ \partial_t h_2 + \partial_x (h_2 u_2) = 0, \\ \partial_t (h_2 u_2) + \partial_x \left(h_2 u_2^2 + g \dfrac{h_2^2}{2} \right) + g \dfrac{\rho_1}{\rho_2} h_2 \partial_x h_1 = -g h_2 \partial_x z, \end{cases} \tag{1}$$

* Corresponding author.
E-mail address: ccabacar@uax.es (C. Caballero-Cárdenas).

https://doi.org/10.1016/j.apnum.2025.07.014
Received 2 June 2025; Received in revised form 22 July 2025; Accepted 26 July 2025

Available online 29 July 2025

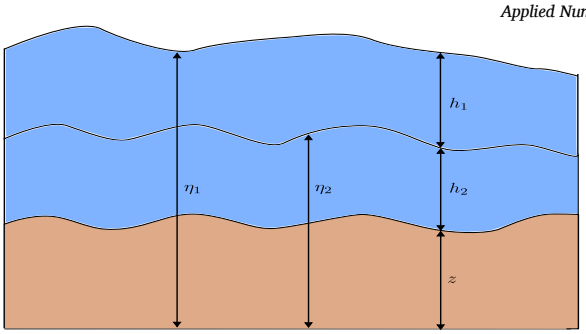

Fig. 1. Sketch of the two-layer shallow water: h_1, h_2 water heights, z topography, η_2 the interface between the fluids and η_1 the free surface.

where $h_1 \geq 0$ and u_1 denote the depth and velocity of the upper layer, and $h_2 \geq 0$ and u_2 are concerned with the lower one (see Fig. 1). Moreover, z is the bottom topography and g is the gravity constant. We shall denote by $q_\alpha = h_\alpha u_\alpha$ the discharge for each layer. The free surface is defined as $\eta_1 = h_1 + h_2 + z$ and $\eta_2 = h_2 + z$ corresponds to the interface between both fluids. The first and third equations indicate the conservation of mass, while the second and fourth equations correspond to the momentum for each layer. A global momentum equation can be obtained by multiplying the second equation by ρ_1, the third one by ρ_2 and adding them together. In fact, that global momentum equation is conservative for flat bottom topography. The two-layer shallow water system is derived by depth averaging the incompressible Navier-Stokes equations under the assumption of hydrostatic and constant density for each layer.

It is important to notice the presence of non-conservative products that couple the two layers whose treatment is subject to nontrivial difficulties (see [23] for instance). As it will be seen below, another difficulty related to the two-layer system is the possible loss of hyperbolicty. In addition, the eigenvalues cannot be expressed by means of easy explicit formulas in general.

These equations can also be reformulated in a more compact way as

$$\partial_t \mathbf{U} + \partial_x \mathbf{F}(\mathbf{U}) + \mathbf{B}(\mathbf{U})\partial_x \mathbf{U} = \mathbf{S}(\mathbf{U})\partial_x z,$$

where $\mathbf{U} = (h_1, h_1u_1, h_2, h_2u_2)^T$ is the vector of unknowns, and

$$\mathbf{F}(\mathbf{U}) = \begin{pmatrix} h_1u_1 \\ h_1u_1^2 + \dfrac{gh_1^2}{2} \\ h_2u_2 \\ h_2u_2^2 + \dfrac{gh_2^2}{2} \end{pmatrix}, \quad \mathbf{B}(\mathbf{U}) = \begin{pmatrix} 0 & 0 & 0 & 0 \\ 0 & 0 & gh_1 & 0 \\ 0 & 0 & 0 & 0 \\ rgh_2 & 0 & 0 & 0 \end{pmatrix},$$

and

$$\mathbf{S}(\mathbf{U}) = \begin{pmatrix} 0 \\ -gh_1 \\ 0 \\ -gh_2 \end{pmatrix}$$

are the flux function, the coupling terms matrix and the source term respectively. It will be also useful to write the equations in the form of a quasi-linear system with a source term

$$\partial_t \mathbf{U} + \mathbf{A}(\mathbf{U})\partial_x \mathbf{U} = \mathbf{S}(\mathbf{U})\partial_x z,$$

where

$$\mathbf{A}(\mathbf{U}) = \frac{\partial \mathbf{F}(\mathbf{U})}{\partial \mathbf{U}} + \mathbf{B}(\mathbf{U}).$$

A few computations show that the characteristic equation of $\mathbf{A}(\mathbf{U})$ is given by

$$(\lambda^2 + u_1^2 - c_1^2 - 2\lambda u_1)(\lambda^2 + u_2^2 - c_2^2 - 2\lambda u_2) = rc_1^2c_2^2,$$

where $r = \dfrac{\rho_1}{\rho_2}$ denotes the ratio of the densities and $c_j = \sqrt{gh_j}$, the sound speed of each layer. In particular, it is easy to see that we have a null eigenvalue when the so called composite Froude number, G, satisfies

$$G^2 = F_1^2 + F_2^2 - (1 - r)F_1^2F_2^2 = 1,$$

where F_j is given by

$$F_j^2 = \frac{u_j^2}{(1-r)c_j^2},$$

which are usually called the internal Froude numbers of each layer. A flow is said to be subcritical when $G^2 < 1$, and supercritical when $G^2 > 1$. In general, for $r > 0$, it is not possible to provide an easy expression for the eigenvalues, although they can be analytically computed using Ferrari's method. If $r = 0$, it is clear that the eigenvalues correspond those of two shallow water system, one for each layer separately. Thus, if $r \approx 0$, the two layers of fluids behave almost independently. However, we are interested in situations in which $r \approx 1$, which often happen in geophysical flows. In this case, the following first-order approximation of the eigenvalues is given in [55]:

$$\lambda_{\text{ext}}^{\pm} = \frac{h_1u_1 + h_2u_2}{h_1 + h_2} \pm \sqrt{g(h_1 + h_2)},$$

$$\lambda_{\text{int}}^{\pm} = \frac{h_1u_1 + h_2u_2}{h_1 + h_2} \pm \sqrt{g(1-r)\frac{h_1h_2}{h_1 + h_2}\left(1 - \frac{(u_1 - u_2)^2}{g_1(h_1 + h_2)}\right)}.$$

Then, based on these first order approximations, it is clear that complex internal eigenvalues will appear when

$$\frac{(u_1 - u_2)^2}{g_1(h_1 + h_2)} > 1,$$

and thus we would lose the hyperbolicity character. This concerns scenarios where the two layers mix, leading to the development of Kelvin-Helmholtz instabilities. In real-world situations, such mixing would result in partial energy dissipation. To replicate this effect in models, friction can be incorporated into the mathematical framework to prevent interface disturbances from escalating and causing inaccuracies in numerical simulations (see [17]). Clearly, in these cases, a more sophisticated model would be necessary. During numerical experiments, the occasional loss of hyperbolicity might be acceptable, provided it does not significantly deviate from the true solution. For additional details on the two-layer shallow water model and issues related to hyperbolicity loss see references [17,18,23,16] and the references therein.

As highlighted in [40], despite these challenges, the two-layer system remains a popular and effective numerical tool for various applications, such as analyzing the flow dynamics in the Strait of Gibraltar—where two streams of differing densities from the Atlantic Ocean and the Mediterranean Sea interact (see [19], for example)—and modeling tsunami generation caused by underwater landslides, which can be approximated as viscous fluids (see [49,31]).

Fully exactly well-balanced property. It is well known that well-balancing is one of the good properties required for any numerical scheme designed to approximate the solution of the systems of balance laws with or without non-conservative products, which is the case we are dealing with. This property means that the scheme should be able to preserve the stationary solutions of the system, or at least a subset of them. This avoids spurious oscillations in the numerical approximations when the solutions are close to a steady state.

In the two-layer shallow water system, the stationary solutions $(h_\alpha)^e$ and $(u_\alpha)^e$ for each layer α are computed by solving the ordinary differential equations

$$\begin{cases} \dfrac{d}{dx}(h_\alpha u_\alpha)^e = 0, \\ \dfrac{d}{dx}\left(h_\alpha u_\alpha^2 + g\dfrac{h_\alpha^2}{2}\right)^e + g r_\alpha h_\alpha^e \partial_x h_\beta^e = -g h_\alpha^e \partial_x z, \end{cases} \tag{2}$$

with $\{\alpha, \beta\} = \{1, 2\}$ and $r_\alpha = (\alpha - 1)r + 2 - \alpha$, which is equivalent to

$$\begin{cases} (h_\alpha u_\alpha)^e = C_{1,\alpha}, \\ \dfrac{(u_\alpha^e)^2}{2} + g(r_\alpha h_\beta^e + h_\alpha^e + z) = C_{2,\alpha}, \end{cases} \tag{3}$$

where $C_{1,\alpha}$ and $C_{2,\alpha}$ are four real constants. A particular case correspond to the so-called lake-at-rest steady states, given by

$$\begin{cases} u_\alpha^e = 0, \quad \alpha = 1, 2, \\ h_1^e = cst., \quad h_2^e + z = cst. \end{cases}$$

Although various definitions of well-balanced schemes can be found in the literature, in this work we adopt those provided in [36]. Accordingly, a scheme is referred to as exactly well-balanced for a steady state if its exact cell averages (or their approximations using a quadrature formula) are preserved by the scheme, whereas it is called well-balanced when it preserves a discrete approximation of them. Moreover, if the scheme preserves every possible steady state, we say that it is fully (exactly) well-balanced.

Many papers deal with the study of well-balanced or fully well-balanced schemes. To name just a few, we refer to [3,38,51,33, 32,6,1,29,2,8] for schemes that only preserve the lake-at-rest steady states, and to [37,10,58,57,4,5,22,48,53,7] for schemes that preserve all the stationary solutions.

Other works dealing with important aspects concerning the two-layer problem are those of [23,20,21,41,45,47,54,52]. To the best of our knowledge, there is no explicit/implicit solver that is exactly fully well-balanced for the two-layer shallow water system.

Splitting and numerical scheme. In line with the philosophy of previous works [25–28], [14], [46], [12], [13], we adopt an operator splitting strategy to solve (1). The idea is to split the pressure and transport terms of the model, leading to an acoustic system and a transport one.

Our numerical scheme will consist in calculating $\mathbf{U}$ by performing first an acoustic step and then the transport one. More precisely and adopting the usual notations in finite volume schemes, we start by defining the constant space step Δx, the time step Δt, the mesh interfaces $x_{i+1/2} = i\Delta x$ for $i \in Z$ and the intermediate times by $t^n = n\Delta t$ for $n \in N$. Then, we denote by $\mathbf{U}_i^n$ an approximation of the average value of the unknown $\mathbf{U}$ on the mesh cell $(x_{i-1/2}, x_{i+1/2})$ at time t^n, and $\mathbf{U}^n$ the vector made of all the $\mathbf{U}_i^n$, for $i \in Z$ (for $n = 0$, $\mathbf{U}_i^0$ is the average on the i-cell of a given initial condition). Our numerical method is thus composed of two stages:

1. Update $\mathbf{U}^n$ to $\mathbf{U}^{n+1-}$ by solving the acoustic system, which will be done either explicitly or implicitly.
2. Exploit $\mathbf{U}^{n+1-}$ to solve the transport system and find $\mathbf{U}^{n+1}$, which will always be done explicitly.

Note that depending on how the acoustic system is solved, we will obtain either fully explicit schemes or semi-implicit ones.

Some splitting strategies similar to this one have already been used in works like [39] for sediment transport and [30] for the two-layer system. The main contribution of the new splitting proposed here in relation to the one that can be found in [30] is that it allows us to obtain a scheme that is, on the one hand, simpler, and on the other hand, fully well-balanced.

Outline. The structure of this paper is outlined as follows: Section 2 is devoted to the acoustic-transport splitting strategy, for which the splitting operator is presented, followed by the study of the two splitting steps. As far as the acoustic step is concerned, the construction of the numerical fluxes is based on that of a relaxed system associated to the acoustic problem, while the source term discretization proposed to obtain the fully exactly well-balanced property is based on the prior construction of stationary solutions. Moreover, we address the additional difficulty of the presence of coupling terms between the layers. Section 3 is devoted to the description of the fully exactly well-balanced reconstruction operators, and Section 4, to the second order extension of the schemes. Finally, in Section 5 different numerical experiments of interest are presented, while in Section 6 some conclusions are drawn.

2. Acoustic-transport splitting

In what follows, we will adopt the acoustic-transport operator splitting strategy described below to solve the two-layer shallow water system, keeping in mind the difficulty due to the presence of the coupling terms between the layers.

The idea is to split the different pressure and transport terms of the model, leading to the so-called acoustic system

$$\begin{cases} \partial_t h_1 = 0, \\ \partial_t (h_1 u_1) + h_1 \partial_x \left(g h_1 + g h_2 \right) = -g h_1 \partial_x z, \\ \partial_t h_2 = 0, \\ \partial_t (h_2 u_2) + h_2 \partial_x \left(g h_2 + r g h_1 \right) = -g h_2 \partial_x z, \end{cases} \tag{4}$$

which also writes for $h_1,\ h_2 > 0$ as

$$\begin{cases} \partial_t h_1 = 0, \\ \partial_t u_1 + \partial_x \left(g h_1 + g h_2 \right) = -g \partial_x z, \\ \partial_t h_2 = 0, \\ \partial_t u_2 + \partial_x \left(g h_2 + r g h_1 \right) = -g \partial_x z, \end{cases} \tag{5}$$

and the transport system

$$\begin{cases} \partial_t h_1 + \partial_x (h_1 u_1) = 0, \\ \partial_t (h_1 u_1) + \partial_x \left(h_1 u_1^2 \right) = 0, \\ \partial_t h_2 + \partial_x (h_2 u_2) = 0, \\ \partial_t (h_2 u_2) + \partial_x \left(h_2 u_2^2 \right) = 0. \end{cases} \tag{6}$$

Our numerical scheme will consist in calculating the solution by solving first the acoustic system (5) and then the transport system (6).

Note that we are considering the non-conservative formulation in the acoustic step. However, we have compared our results with other standard schemes in test 5.1 and no significant differences have been observed. Of course, we cannot expect to converge to the same weak solution, but this discussion is out of the scope of this work. In fact, the characterization of weak solutions is one of the main challenges concerning the two-layer shallow water equations. Moreover, we have numerically checked that the total mass and the total momentum in the flat bottom case are preserved up to machine accuracy.

2.1. Acoustic step

In the finite volume framework, the key point in the design of a numerical scheme for (5) is the definition of a numerical flux function at interfaces to evaluate the pressure terms, as well as a suitable evaluation of the source term $g\partial_x z$. In order to address these two difficulties sequentially, the preliminary step will be to consider the case of flat topography and define the numerical fluxes. Thereafter, the non-flat bottom case will be considered, and a discretization for the source term will be obtained, so we can achieve the fully exactly well-balanced property.

2.1.1. Flat topography case

The homogeneous system associated to (5) is

$$\begin{cases} \partial_t h_1 = 0, \\ \partial_t u_1 + \partial_x \left(g h_1 + g h_2 \right) = 0, \\ \partial_t h_2 = 0, \\ \partial_t u_2 + \partial_x \left(g h_2 + r g h_1 \right) = 0. \end{cases} \tag{7}$$

Relaxation approximation. In order to define the numerical fluxes at interfaces to evaluate gh_1 and gh_2, we introduce the following relaxation linearization of the previous evolution equations on u_1 and u_2, namely

$$\begin{cases} \partial_t C_1 + a_1^2 \partial_x u_1 = 0, \\ \partial_t u_1 + \partial_x \left(C_1 + C_2 \right) = 0, \\ \partial_t C_2 + a_2^2 \partial_x u_2 = 0. \\ \partial_t u_2 + \partial_x \left(C_2 + r C_1 \right) = 0, \end{cases} \tag{8}$$

where a_1 and a_2 are constants satisfying the subcharacteristic condition given by

$$a_i \geq \sqrt{g(h_1 + h_2)}, \quad i = 1, 2, \tag{9}$$

and the relaxation variables C_1 and C_2 are such that

$$\lim_{\lambda \to \infty} C_i = g h_i, \quad i = 1, 2.$$

Note that the subcharacteristic condition is approximately obtained considering the barotropic component of the two-layer shallow water system, that behaves like a single-layer shallow water system (see for example [9] and [13]).

The matrix associated to this system is given by

$$\begin{pmatrix} 0 & a_1^2 & 0 & 0 \\ 1 & 0 & 1 & 0 \\ 0 & 0 & 0 & a_2^2 \\ r & 0 & 1 & 0 \end{pmatrix},$$

which has eigenvalues

$$\lambda_E^{\pm} = \pm \sqrt{\frac{a_1^2 + a_2^2 + d}{2}},$$

$$\lambda_I^{\pm} = \pm \sqrt{\frac{a_1^2 + a_2^2 - d}{2}},$$

where

$$d = \sqrt{\left(a_1^2 - a_2^2\right)^2 + 4 r a_1^2 a_2^2},$$

and the matrix of eigenvectors is given by

$$K = \begin{pmatrix} a_1^2 a_2^2 & a_1^2 a_2^2 & a_1^2 a_2^2 & a_1^2 a_2^2 \\ -\lambda_E a_2^2 & -\lambda_I a_2^2 & \lambda_I a_2^2 & \lambda_E a_2^2 \\ a_2^2 \left(\lambda_E^2 - a_1^2\right) & a_2^2 \left(\lambda_I^2 - a_1^2\right) & a_2^2 \left(\lambda_I^2 - a_1^2\right) & a_2^2 \left(\lambda_E^2 - a_1^2\right) \\ -\lambda_E \left(\lambda_E^2 - a_1^2\right) & -\lambda_I \left(\lambda_I^2 - a_1^2\right) & \lambda_I \left(\lambda_I^2 - a_1^2\right) & \lambda_E \left(\lambda_E^2 - a_1^2\right) \end{pmatrix},$$

where we are denoting $\lambda_E = \lambda_E^+$ and $\lambda_I = \lambda_I^+$ to simplify the notation. The inverse of the matrix of eigenvectors is

$$K^{-1} = \frac{1}{2 a_1^2 a_2^2 \lambda_I \lambda_E (\lambda_E^2 - \lambda_I^2)} \begin{pmatrix} \lambda_I \lambda_E (a_1^2 - \lambda_I^2) & -a_1^2 \lambda_I (a_1^2 - \lambda_I^2) & a_1^2 \lambda_I \lambda_E & -a_1^2 a_2^2 \lambda_I \\ -\lambda_I \lambda_E (a_1^2 - \lambda_E^2) & a_1^2 \lambda_E (a_1^2 - \lambda_E^2) & -a_1^2 \lambda_I \lambda_E & a_1^2 a_2^2 \lambda_E \\ -\lambda_I \lambda_E (a_1^2 - \lambda_E^2) & -a_1^2 \lambda_E (a_1^2 - \lambda_E^2) & -a_1^2 \lambda_I \lambda_E & -a_1^2 a_2^2 \lambda_E \\ \lambda_I \lambda_E (a_1^2 - \lambda_I^2) & a_1^2 \lambda_I (a_1^2 - \lambda_I^2) & a_1^2 \lambda_I \lambda_E & a_1^2 a_2^2 \lambda_I \end{pmatrix}.$$

It is interesting to note that the proposed relaxed system has always real eigenvalues given by explicit easy formulas.

If we now multiply the inverse matrix by the vector of variables $(C_1, u_1, C_2, u_2)^T$, we obtain the Riemann invariants that we denote by $(R_{+E}, R_{+I}, R_{-I}, R_{-E})$, namely

$$\begin{pmatrix} R_{-E} \\ R_{-I} \\ R_{+I} \\ R_{+E} \end{pmatrix} = K^{-1} \begin{pmatrix} C_1 \\ u_1 \\ C_2 \\ u_2 \end{pmatrix}. \tag{10}$$

Of course, C_1, u_1, C_2, u_2 can be recovered from

$$\begin{pmatrix} C_1 \\ u_1 \\ C_2 \\ u_2 \end{pmatrix} = K \begin{pmatrix} R_{-E} \\ R_{-I} \\ R_{+I} \\ R_{+E} \end{pmatrix}, \tag{11}$$

while the equations that the Riemann invariants satisfy are just simple transport equations,

$$\begin{cases} \partial_t R_{-E} - \lambda_E \partial_x R_{-E} = 0, \\ \partial_t R_{-I} - \lambda_I \partial_x R_{-I} = 0, \\ \partial_t R_{+I} + \lambda_I \partial_x R_{+I} = 0, \\ \partial_t R_{+E} + \lambda_E \partial_x R_{+E} = 0, \end{cases} \tag{12}$$

which can be solved explicitly or implicitly.

Numerical discretization of the homogeneous acoustic system. We propose the following discretization of the acoustic system (4) without topography, i.e. neglecting the source term,

$$\begin{cases} (h_1)_i^{n+1-} = (h_1)_i^n, \\ (h_1 u_1)_i^{n+1-} = (h_1 u_1)_i^n - (h_1)_i^n \dfrac{\Delta t}{\Delta x} \left((C_1)_{i+1/2}^{\#} + (C_2)_{i+1/2}^{\#} - (C_1)_{i-1/2}^{\#} - (C_2)_{i-1/2}^{\#} \right), \\ (h_2)_i^{n+1-} = (h_2)_i^n, \\ (h_2 u_2)_i^{n+1-} = (h_2 u_2)_i^n - (h_2)_i^n \dfrac{\Delta t}{\Delta x} \left((C_2)_{i+1/2}^{\#} + r(C_1)_{i+1/2}^{\#} - (C_2)_{i-1/2}^{\#} - r(C_1)_{i-1/2}^{\#} \right), \end{cases}$$

where $\# = n$ for an explicit scheme and $\# = n+1-$ for an implicit one and the numerical fluxes are defined from the Riemann invariants by

$$\begin{pmatrix} (C_1)_{i+1/2}^{\#} \\ (u_1)_{i+1/2}^{\#} \\ (C_2)_{i+1/2}^{\#} \\ (u_2)_{i+1/2}^{\#} \end{pmatrix} = K \begin{pmatrix} (R_{-E})_{i+1}^{\#}(x_{i+1/2}) \\ (R_{-I})_{i+1}^{\#}(x_{i+1/2}) \\ (R_{+I})_i^{\#}(x_{i+1/2}) \\ (R_{+E})_i^{\#}(x_{i+1/2}) \end{pmatrix}, \tag{13}$$

where we use the appropriate reconstructions of the different Riemann invariants, taking into account their direction of propagation of the information.

The values of the Riemann invariants at time $n+1-$ are obtained by solving system (12), which is composed of four transport equations with given constant velocities $\pm\lambda_I$ and $\pm\lambda_E$, whose solutions can be approximated by the classical upwind formulas

$$\begin{cases} (R_{-E})_i^{n+1-} = (R_{-E})_i^n + \lambda_E \dfrac{\Delta t}{\Delta x} \left((R_{-E})_{i+1}^{n+1-}(x_{i+1/2}) - (R_{-E})_i^{n+1-}(x_{i-1/2}) \right), \\ (R_{-I})_i^{n+1-} = (R_{-I})_i^n + \lambda_I \dfrac{\Delta t}{\Delta x} \left((R_{-I})_{i+1}^{n+1-}(x_{i+1/2}) - (R_{-I})_i^{n+1-}(x_{i-1/2}) \right), \\ (R_{+I})_i^{n+1-} = (R_{+I})_i^n - \lambda_I \dfrac{\Delta t}{\Delta x} \left((R_{+I})_i^{n+1-}(x_{i+1/2}) - (R_{+I})_{i-1}^{n+1-}(x_{i-1/2}) \right), \\ (R_{+E})_i^{n+1-} = (R_{+E})_i^n - \lambda_E \dfrac{\Delta t}{\Delta x} \left((R_{+E})_i^{n+1-}(x_{i+1/2}) - (R_{+E})_{i-1}^{n+1-}(x_{i-1/2}) \right). \end{cases} \tag{14}$$

2.1.2. Non-flat topography case

Concerning the whole system (4), it is crucial to pay particular attention to the discretization of the source term $-g\partial_x z$ in order to obtain the fully exactly well-balanced property.

A natural way to do this starts from considering an equilibrium or stationary solution. The stationary solutions $(h_\alpha)^e$ and $(u_\alpha)^e$ for each layer α are computed by solving (3). More precisely, the equilibrium solution computed on cell i and denoted $(h_\alpha)_i^e$ and $(u_\alpha)_i^e$ will be computed by choosing the constants $C_{1,\alpha}$ and $C_{2,\alpha}$ with the values at the center of the cells. In practice, a Newton-Raphson algorithm is used to do this. The system solved to obtain this stationary solution is described in Appendix A.

It is important to note that the stationary solution used in both the implicit and the explicit schemes is always computed using the solution at time step n. This approach is adopted in order to avoid solving the nonlinear problems that would arise from considering the stationary solution at a different time.

Another relevant point to highlight is that the computations are local to each stencil. In the case of the first-order scheme, the stationary solution only needs to be determined within a single cell: the central value is known, and it is only necessary to compute the stationary values at the intercells. For second-order schemes, the stationary problems remain local to the stencil, but in this case one must determine the values at the intercells as well as the cell centers in the neighboring cells. See, for instance [36,34,12,11].

As is often the case, the transition through a critical state may lead to certain difficulties. Nonetheless, addressing these issues lies beyond the scope of the present work.

Now, in order to include the source terms we follow a similar procedure as the one proposed in [13], integrating equation (2) over the cell $[x_{i-1/2}, x_{i+1/2}]$. Then, taking into account the splitting procedure, system (5) can be recast as

$$\begin{cases} \partial_t h_1 = 0, \\ \partial_t u_1 + \partial_x \left(g h_1 - g h_1^e + g h_2 - g h_2^e \right) = 0, \\ \partial_t h_2 = 0, \\ \partial_t u_2 + \partial_x \left(g h_2 - g h_2^e + r g h_1 - r g h_1^e \right) = 0. \end{cases} \tag{15}$$

Now, considering (8), we add the equilibrium terms $(C_1)_i^e = g(h_1)_i^e$ and $(C_2)_i^e = g(h_2)_i^e$ computed from the reconstructed stationary solutions $(h_1)_i^e$ and $(h_2)_i^e$ of each layer on cell i, resulting on the following scheme

$$\begin{cases} (h_1)_i^{n+1-} = (h_1)_i^n, \\ (h_1 u_1)_i^{n+1-} = (h_1 u_1)_i^n - (h_1)_i^n \dfrac{\Delta t}{\Delta x} \left((C_1 + C_2)_{i+1/2}^{\#} - (C_1 + C_2)_{i-1/2}^{\#} \right) \\ \qquad\qquad + (h_1)_i^n \dfrac{\Delta t}{\Delta x} \left((C_1 + C_2)_i^e (x_{i+1/2}) - (C_1 + C_2)_i^e (x_{i-1/2}) \right), \\ (h_2)_i^{n+1-} = (h_2)_i^n, \\ (h_2 u_2)_i^{n+1-} = (h_2 u_2)_i^n - (h_2)_i^n \dfrac{\Delta t}{\Delta x} \left((C_2 + r C_1)_{i+1/2}^{\#} - (C_2 + r C_1)_{i-1/2}^{\#} \right) \\ \qquad\qquad + (h_2)_i^n \dfrac{\Delta t}{\Delta x} \left((C_2 + r C_1)_i^e (x_{i+1/2}) - (C_2 + r C_1)_i^e (x_{i-1/2}) \right). \end{cases} \tag{16}$$

Analogously, equation (14) should also be modified to ensure the fully exactly well-balanced property, giving

$$\begin{cases} (R_{-E})_i^{n+1-} = (R_{-E})_i^n + \lambda_E \dfrac{\Delta t}{\Delta x} \left((R_{-E})_{i+1}^{n+1-} (x_{i+1/2}) - (R_{-E})_i^{n+1-} (x_{i-1/2}) \right) \\ \qquad\qquad - \lambda_E \dfrac{\Delta t}{\Delta x} \left((R_{-E})_{i+1}^e (x_{i+1/2}) - (R_{-E})_i^e (x_{i-1/2}) \right), \\ (R_{-I})_i^{n+1-} = (R_{-I})_i^n + \lambda_I \dfrac{\Delta t}{\Delta x} \left((R_{-I})_{i+1}^{n+1-} (x_{i+1/2}) - (R_{-I})_i^{n+1-} (x_{i-1/2}) \right) \\ \qquad\qquad - \lambda_I \dfrac{\Delta t}{\Delta x} \left((R_{-I})_{i+1}^e (x_{i+1/2}) - (R_{-I})_i^e (x_{i-1/2}) \right), \\ (R_{+I})_i^{n+1-} = (R_{+I})_i^n - \lambda_I \dfrac{\Delta t}{\Delta x} \left((R_{+I})_i^{n+1-} (x_{i+1/2}) - (R_{+I})_{i-1}^{n+1-} (x_{i-1/2}) \right) \\ \qquad\qquad + \lambda_I \dfrac{\Delta t}{\Delta x} \left((R_{+I})_i^e (x_{i+1/2}) - (R_{+I})_{i-1}^e (x_{i-1/2}) \right), \\ (R_{+E})_i^{n+1-} = (R_{+E})_i^n - \lambda_E \dfrac{\Delta t}{\Delta x} \left((R_{+E})_i^{n+1-} (x_{i+1/2}) - (R_{+E})_{i-1}^{n+1-} (x_{i-1/2}) \right) \\ \qquad\qquad + \lambda_E \dfrac{\Delta t}{\Delta x} \left((R_{+E})_i^e (x_{i+1/2}) - (R_{+E})_{i-1}^e (x_{i-1/2}) \right). \end{cases} \tag{17}$$

If a steady state initial condition is considered, that is $(R_{\pm E})_i^0 = (R_{\pm E})_i^e$ and $(R_{\pm I})_i^0 = (R_{\pm I})_i^e$, then $(R_{\pm E})_i^{1-} = (R_{\pm E})_i^e$ and $(R_{\pm I})_i^{1-} = (R_{\pm I})_i^e$ is a solution of system (17). In addition, in (16) we would have that $(C_1 + C_2)_{i\pm1/2}^{\#} = (C_1 + C_2)_{i\pm1/2}^e (x_{i\pm1/2})$ and $(C_2 + rC_1)_{i\pm1/2}^{\#} = (C_2 + rC_1)_{i\pm1/2}^e (x_{i\pm1/2})$ resulting on $(h_1)_i^{1-} = (h_1)_i^0$, $(h_2)_i^{1-} = (h_2)_i^0$, $(h_1 u_1)_i^{1-} = (h_1 u_1)_i^0$ and $(h_2 u_2)_i^{1-} = (h_2 u_2)_i^0$, as desired.

Finally, let us remark that the CFL condition related to the pressure step, if it is done explicitly, is given by

$$\Delta t \leq \frac{\Delta x \cdot \mathrm{CFL}_p}{\lambda_E^+}. \tag{18}$$

2.2. Transport step

It remains to describe the discretization of the transport step, which is naturally given by

$$(X_\alpha)_i^{n+1} = (X_\alpha)_i^{n+1-} - \frac{\Delta t}{\Delta x} \left((u_\alpha)_{i+1/2}^{n+1-} (X_\alpha)_{i+1/2}^{n+1-} - (u_\alpha)_{i-1/2}^{n+1-} (X_\alpha)_{i-1/2}^{n+1-} \right), \tag{19}$$

for $\alpha = 1, 2$, $X = h, hu$, and for all i

$$(X_\alpha)_{i+1/2}^{n+1-} = \begin{cases} (X_\alpha)_i^{n+1-}(x_{i+1/2}) & \text{if} \quad (u_\alpha)_{i+1/2}^{n+1-} \geq 0, \\ (X_\alpha)_{i+1}^{n+1-}(x_{i+1/2}) & \text{if} \quad (u_\alpha)_{i+1/2}^{n+1-} < 0, \end{cases}$$

where the values $(X_\alpha)_i^{n+1-}(x_{i+1/2})$ and $(X_\alpha)_{i+1}^{n+1-}(x_{i+1/2})$ are computed using the appropriate fully exactly well-balanced reconstruction operator as it will be described in Section 3. It is essential to consider these fully exactly well-balanced reconstruction operators in the transport step in order to obtain the fully exactly well-balanced property. See, for instance, [11,13] for more detail.

The CFL condition associated to this step is given by

$$\Delta t \leq \frac{\Delta x \cdot \mathrm{CFL}_t}{\max_i(|(u_1)_i|, |(u_2)_i|)}. \tag{20}$$

It is important to clarify that for explicit schemes, the time step Δt will be chosen as the minimum value satisfying the conditions expressed in equations (18) and (20). When the acoustic system is solved implicitly, only (20) will be required. In many applications, for small Froude number, it is expected that (18) is much more restrictive than (20). Therefore, when applying the semi-implicit approach, we will usually consider a CFL number greater than 1, meaning that we compute Δt by (18) for this CFL number. However, one must bear in mind that our semi-implicit schemes are still subject to a stability limitation from the transport step, which depends on the fluid velocity. As a result, although the constraint linked to the sound speed is relaxed in the implicit treatment, the time step cannot be arbitrarily large, since it remains bounded by (20).

3. Fully exactly well-balanced space reconstruction operators

This section is devoted to the construction of first and second order fully well-balanced reconstruction operators. We begin by detailing the procedure used to derive fully exactly well-balanced operators for the explicit schemes. We then proceed to develop the corresponding operators for the implicit formulations.

Fully exactly well-balanced space reconstruction operator for explicit schemes. We begin by defining a suitable space reconstruction operator. Note that the objective is to increase the order of accuracy in space, while keeping the well-balanced property of our schemes. We follow the general strategy presented in [24], combined with the ideas introduced in [12]. The first step is to define, from a given set of constant cell values $\{\mathbf{U}_i^n\}$ on each cell $I_i = (x_{i-1/2}, x_{i+1/2})$, an exact fully exactly well-balanced reconstruction operator. For each i, it consists on

1. Finding, if possible, a stationary solution $x \mapsto \mathbf{U}_i^e(x)$ such that

$$\frac{1}{\Delta x} \int_{x_{i-1/2}}^{x_{i+1/2}} \mathbf{U}_i^e(x)\, dx = \mathbf{U}_i^n.$$

   Otherwise, take $\mathbf{U}_i^e \equiv 0$.
2. Computing the fluctuations $\{\mathbf{V}_j^n\}_{j \in S_i}$, given by

$$\mathbf{V}_j^n = \mathbf{U}_j^n - \frac{1}{\Delta x} \int_{x_{j-1/2}}^{x_{j+1/2}} \mathbf{U}_i^e(x)\, dx, \quad j \in S_i,$$

   where S_i is a given stencil of cell I_i.
3. Applying a standard reconstruction operator of order p, denoted by $\mathbf{Q}_i$, to the fluctuations,

$$\mathbf{Q}_i^n(x) = \mathbf{Q}_i(x; \{\mathbf{V}_j^n\}_{j \in S_i}).$$

4. Finally, defining the fully exactly well-balanced reconstruction operator as

$$\mathbf{P}_i^n(x) = \mathbf{U}_i^e(x) + \mathbf{Q}_i^n(x).$$

Note that, in practice, a quadrature formula will be used to evaluate the integrals. As only first and second order reconstruction operators are considered here, the integrals are approximated by the mid-point rule, so that the stationary solutions are such that

$$\mathbf{U}_i^e(x_i) = \mathbf{U}_i^n$$

in step 1 above, and

$$\mathbf{V}_j^n = \mathbf{U}_j^n - \mathbf{U}_i^e(x_j), \quad j \in S_i,$$

in step 2.

The proposed reconstruction operator described in this section will be applied in a classical way to the computations of the numerical fluxes at interfaces $i+1/2$ in update formulas (13) and (16), when the schemes are explicit in time, that is to say when $\# = n$, and in the transport step (19).

Fully exactly well-balanced space reconstruction operator for implicit schemes. When considering implicit schemes such that $\# = n+1-$, a similar approach would be very costly and therefore out of reach in practice since it implies the computation of stationary solutions at every cell from the solution at time $n+1-$ that we do not know.

In order to avoid this, we suggest to proceed as in [12]. The fully exactly well-balanced reconstruction operator defined by step 4 above, namely

$$\mathbf{P}_i^n(x) = \mathbf{U}_i^e(x) + \mathbf{Q}_i(x; \{\mathbf{V}_j^n\}_{j\in\mathcal{S}_i}),$$

is replaced by a standard reconstruction operator based on time fluctuations, namely

$$\mathbf{P}_i^n(x,t) = \mathbf{P}_i^n(x) + \tilde{\mathbf{Q}}_i(x; \{\mathbf{U}_j^{t,f}\}_{j\in\mathcal{S}_i}), \quad \text{where} \quad \mathbf{U}_j^{t,f} = \mathbf{U}_j(t) - \mathbf{U}_j^n.$$

If we consider a first-order reconstruction, the reconstruction operator can be written as

$$\mathbf{P}_i^n(x,t) = \mathbf{U}_i^e(x) + \mathbf{U}_i^n - \mathbf{U}_i^e(x_i) + \mathbf{U}_i(t) - \mathbf{U}_i^n.$$

If we consider a second-order reconstruction, the reconstruction operator can be written as

$$\mathbf{P}_i^n(x,t) = \mathbf{U}_i^e(x) + \mathbf{U}_i^n - \mathbf{U}_i^e(x_i) + \Delta\mathbf{V}_i^n(x-x_i) + \mathbf{U}_i(t) - \mathbf{U}_i^n + \Delta\mathbf{U}_i^{n,f}(x-x_i),$$

where $\Delta\mathbf{V}_i^n$ are the space fluctuations with respect to the stationary solution frozen at time t^n, and $\Delta\mathbf{U}_i^{n,f}$ are the time fluctuations.

Here, $\Delta\mathbf{V}_i^n$ is computed using the avg limiter [44], that is,

$$\Delta\mathbf{V}_i^n = \frac{1}{\Delta x}\left(\phi_{i+}^n(\mathbf{V}_i^n - \mathbf{V}_{i-1}^n) + \phi_{i-}^n(\mathbf{V}_{i+1}^n - \mathbf{V}_i^n)\right),$$

with

$$\phi_{i-}^{t_0} = \begin{cases} \dfrac{|d_{i-}|}{|d_{i-}| + |d_{i+}|} & \text{if } |d_{i-}| + |d_{i+}| > 0, \\ 0 & \text{otherwise,} \end{cases}$$

and

$$\phi_{i+}^{t_0} = \begin{cases} \dfrac{|d_{i+}|}{|d_{i-}| + |d_{i+}|} & \text{if } |d_{i-}| + |d_{i+}| > 0, \\ 0 & \text{otherwise,} \end{cases}$$

where $d_{i-} = \mathbf{V}_i^n - \mathbf{V}_{i-1}^n$ and $d_{i+} = \mathbf{V}_{i+1}^n - \mathbf{V}_i^n$.

Moreover, $\Delta\mathbf{U}_i^{t,f}$ is computed as

$$\Delta\mathbf{U}_i^{t,f} = \frac{1}{\Delta x}\left(\tilde{\phi}_{i+}^{t_0}(\mathbf{U}_i^{t,f} - \mathbf{U}_{i-1}^{t,f}) + \tilde{\phi}_{i-}^{t_0}(\mathbf{U}_{i+1}^{t,f} - \mathbf{U}_i^{t,f})\right)$$

with $\tilde{\phi}_{i\pm}^{t_0} = \phi_{i\pm}^{t_0}$. Note that in both cases we have used the same limiter computed at time t^n to avoid nonlinearities.

The proposed reconstruction operator described in this section is then applied in a classical way to the computations of the numerical fluxes at interfaces $i+1/2$ when the schemes are now implicit in time, that is to say when $\# = n+1-$.

4. Second-order in time extension

In order to obtain second-order accuracy in time and space, we use a second-order time integration method based on Strang splitting (see [56,42,43]) combined with the previous second-order space reconstructions.

To be more precise, the following sequence of sub-steps is applied at each time iteration:

1. Perform a half time step $\Delta t/2$ of the acoustic (resp. transport) system, yielding intermediate approximations $\widetilde{h}_i^{n+1}$ and $\widetilde{(hu)}_i^{n+1}$.
2. Advance the transport (resp. acoustic) system using a full time step Δt, obtaining the approximations $\widehat{h}_i^{n+1}$ and $\widehat{(hu)}_i^{n+1}$.
3. Conclude with another half time step $\Delta t/2$ of the acoustic (resp. transport) system, resulting in the final values h_i^{n+1} and $(hu)_i^{n+1}$ at time t^{n+1}.

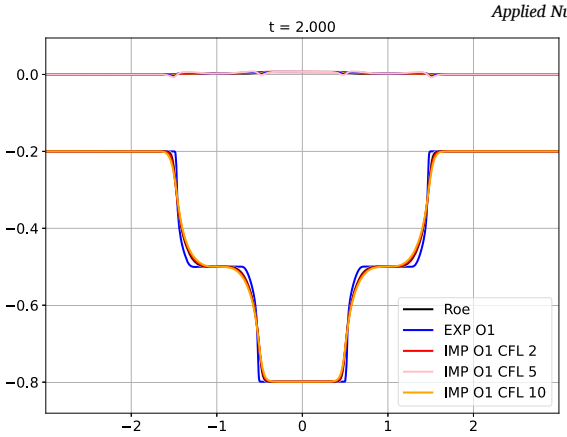

Fig. 2. Free surface, η_1, and interface, η_2, obtained at time $t = 2$ for a shock test case: comparison between Roe, EXP O1 and IMP O1 schemes. (For interpretation of the colors in the figure(s), the reader is referred to the web version of this article.)

It is worth noting that, in principle, either of the two possible orderings in the splitting procedure may be adopted. That is, one could perform the pressure–transport–pressure or transport–pressure–transport steps. In this work, we choose the latter, as this ordering was observed to provide improved stability properties in the previous work [12].

5. Numerical experiments

In this section we will check and compare the properties and performance of four different schemes: first and second order explicit schemes, in which both the pressure step and the transport step are performed explicitly, and first and second order semi-implicit schemes, in which the pressure step is solved implicitly while the transport one is done explicitly. We will refer to them as EXP O1, EXP O2, IMP O1, IMP O2, respectively.

5.1. Comparison with a standard path-conservative Roe's scheme

Let us perform first a comparison between the schemes introduced in this paper and a standard path-conservative Roe's solver based on segment paths (see [50] and [15]). In order to do so, we consider an initial condition that introduces a discontinuity in the height of the second layer h_2, while setting $q_1 = q_2 = 0$ and assuming a flat bottom topography. The initial condition is then given by:

$$h_1(x,t=0) = 1 - h_2(x,t=0), \quad h_2(x,t=0) = \begin{cases} 0.8, & x < -1, \\ 0.2, & -1 <= x <= 1, \\ 0.8, & x > 1, \end{cases}$$

$$q_1(x,t=0) = q_2(x,t=0) = 0,$$

together with $r = 0.98$.

Figs. 2, 3 and 4 present the solutions obtained using a Roe-type scheme with CFL 0.5 and 3000 cells (used as a reference solution) and our proposed first-order schemes: the explicit scheme (EXP O1) with CFL 0.9 and the implicit scheme (IMP O1) for various CFL numbers (CFL = 2, 5, 10) using for both 200 cells.

We observe that both the EXP O1 and IMP O1 schemes are able to reproduce the general structure of the reference Roe-type solution. All schemes capture the amplitude and shape of the shock well, with the implicit schemes showing slightly more diffusive behavior as the CFL number increases, as expected. However, even for high CFL numbers (e.g., CFL = 10), the IMP O1 scheme results are quite good.

A closer view of the solution for η_2 in Fig. 3 helps to evaluate the resolution of the shock front. The Roe scheme exhibits the sharpest profile, while the explicit and low-CFL implicit schemes (CFL = 2) follow it closely. As the CFL number increases, the IMP O1 scheme becomes slightly more diffusive, yet the shock position and overall profile remain consistent with the reference.

The results for the discharges q_1 and q_2 in Fig. 4, further confirm the good performance of our methods. All schemes present the same behavior, including the symmetry and localization of the velocity-induced waves. Again, the Roe scheme is slightly sharper, but the explicit and implicit schemes provide comparable results with only minor differences. The implicit scheme maintains accuracy even for large CFL numbers, demonstrating its potential for more efficient simulations with larger time steps.

In addition to the qualitative agreement with the Roe-type reference solution, we have also verified that the schemes used for this test preserve the total mass and momentum, obtaining that they remain constant throughout the simulation with deviations on the order of 10^{-16}. This excellent behavior further supports the reliability of the proposed methods, even when large time steps are employed in the implicit schemes.

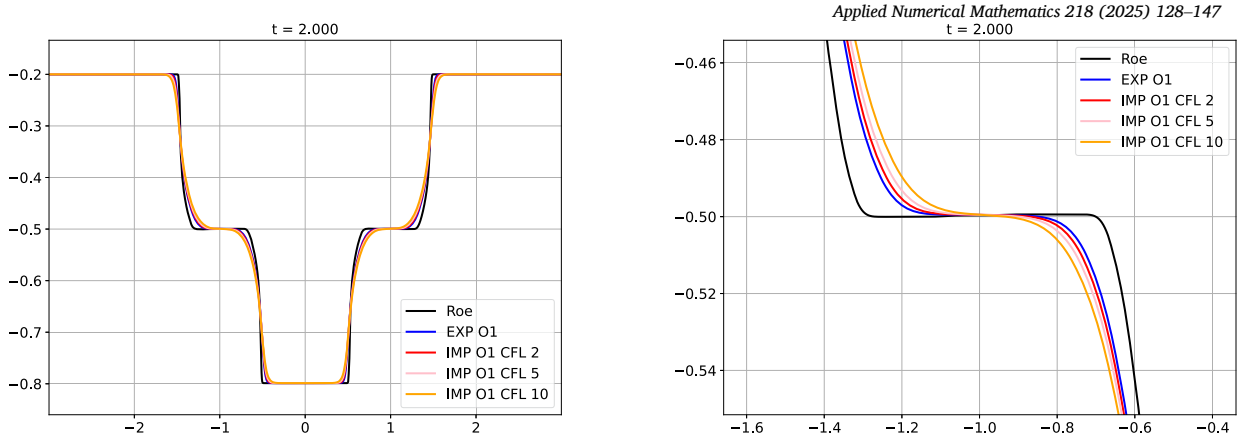

(a) η_2 (b) η_2 (zoom)

Fig. 3. Details on the interface, η_2, obtained at time $t = 2$ for a shock test case: comparison between Roe, EXP O1 and IMP O1 schemes.

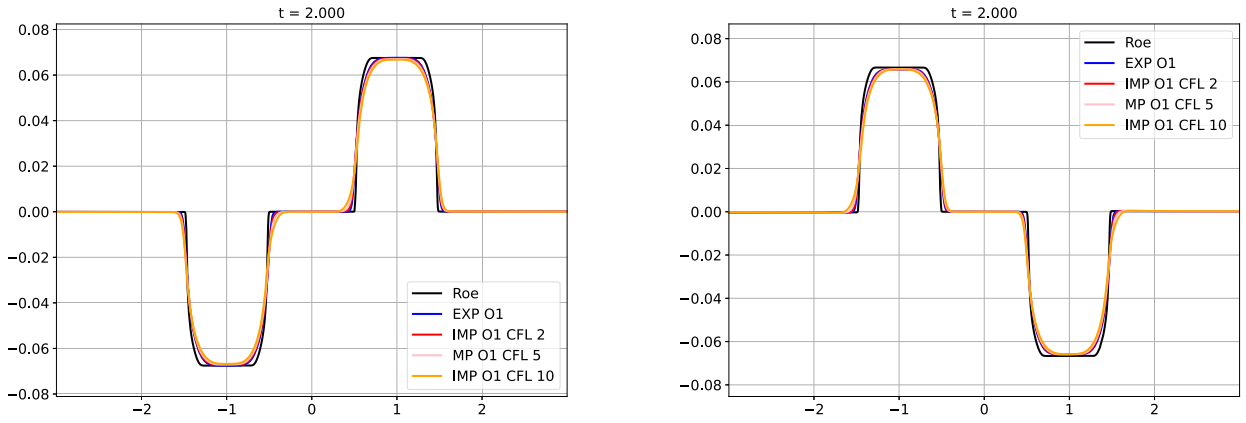

(a) q_1 (b) q_2

Fig. 4. Discharges obtained at time $t = 2$ for a shock test case: comparison between Roe, EXP O1 and IMP O1 schemes.

5.2. *Exactly well-balanced property check: lake-at-rest*

Let us consider a lake-at-rest initial condition in the domain $[-5, 5]$ given by the following topography:

$$z(x) = -1 + 0.1e^{-x^2}, \tag{21}$$

as well as the water heights and discharges given by

$$\begin{aligned} &h_1(x, t = 0) = 0.2, \quad h_2(x, t = 0) = 0.2 - z(x), \\ &q_1(x, t = 0) = q_2(x, t = 0) = 0. \end{aligned} \tag{22}$$

Moreover, r has been set to be 0.98. This initial condition has been plotted in Fig. 5.

Table 1 shows the errors obtained in L^1-norm for the different schemes when comparing the initial condition with the ones obtained at $t = 1$ using 200 cells. For the explicit schemes, the CFL has been set to 0.9, and for the implicit ones, CFL 5 has been considered. As expected, the lake-at-rest initial condition is preserved up to machine precision.

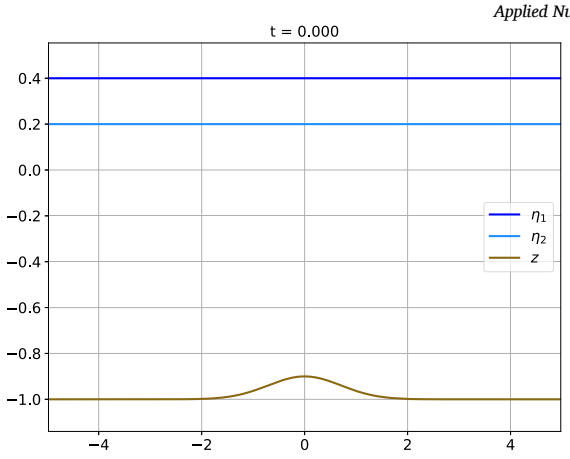

Fig. 5. Lake-at-rest steady state.

Table 1
Errors in L^1-norm for the solutions obtained for different schemes at time $t = 1$ when compared with the lake-at-rest initial condition.

	Error h_1	Error h_2	Error q_1	Error q_2
EXP O1	3.38e-13	3.54e-13	8.48e-14	3.70e-13
EXP O2	2.86e-13	2.89e-13	7.63e-14	2.57e-13
IMP O1	6.89e-13	7.19e-13	1.55e-13	6.59e-13
IMP O2	4.07e-13	4.85e-13	1.70e-13	7.03e-13

5.3. Fully exactly well-balanced property check: nonzero velocity steady state

To verify the fully exactly well-balanced property of our scheme, a steady state with nonzero velocity has been considered as the initial condition. For this purpose, the same spatial domain of the previous test has been used, along with the same topography (21). The steady state has been computed using the following initial values:

$$\begin{aligned} &q_1(x,t=0)=0.01, \quad q_2(x,t=0)=0.001, \quad x\in[-5,5],\\ &h_1(-5,t=0)=0.005, \quad h_2(-5,t=0)=0.7, \end{aligned} \tag{23}$$

and the remaining values in the domain have been determined accordingly. The resulting steady state has Froude number 4.07, so we are in the case of a supercritical stationary solution. The initial surface η_1 and interface η_2 are shown in Fig. 6. Table 2 shows the errors obtained in L^1-norm for the different schemes when comparing the initial condition with the ones obtained at $t = 1$ using 200 cells. It is confirmed that the fully exactly well-balanced property is satisfied, as expected.

5.4. Accuracy test

Let us now evaluate the order of accuracy of the schemes. To this end, we take as the initial condition a small perturbation of a steady-state configuration where the water is at rest:

$$h_1(x,0)=\begin{cases} 0.05\left(1+\cos\left(\frac{2\pi(x-4750)}{3500}\right)\right) & \text{for} \quad 3000<x<6500\\ 0.05\left(-\left(1+\cos\left(\frac{2\pi(x-9250)}{3500}\right)\right)\right) & \text{for} \quad 7500<x<11000\\ 0 & \text{otherwise,}\end{cases}$$

with $h_2(x,0)=1-z(x)$, $q_1(x,0)=q_2(x,0)=0$, $r=0.98$ and bottom topography

$$z(x)=-\left(50-\exp\left(-\frac{(x-7000)^2}{1000000}\right)\right).$$

The computational domain extends over $[0, 14000]$, and the simulation runs until the final time $t = 1$. We impose periodic boundary conditions. The considered reference solution has 3200 cells. The initial free surface and interfaces are shown in Fig. 7.

The errors and the convergence rates obtained with the different schemes are the expected ones and they are shown in Tables 3-6.

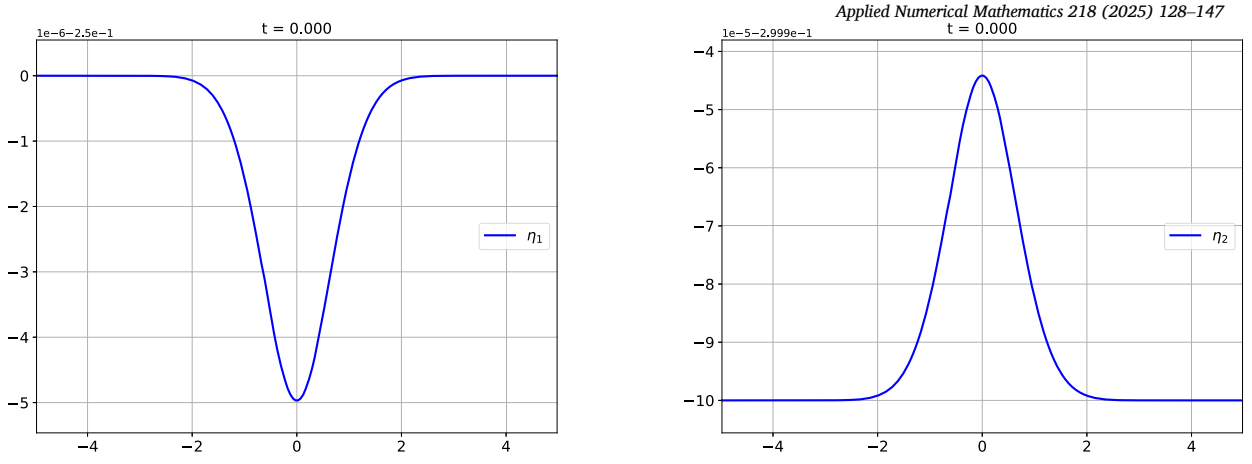

(a) η_1 (b) η_2

Fig. 6. Initial surface η_1 and interface η_2 for the supercritical steady state given by (23).

Table 2
Errors in L^1-norm for the solutions obtained for different schemes at time $t = 1$ when compared with the stationary initial condition given by (23).

	Error h_1	Error h_2	Error q_1	Error q_2
EXP O1	1.96e-13	2.00e-13	2.07e-14	2.19e-13
EXP O2	1.83e-13	1.84e-13	1.79e-14	1.71e-13
IMP O1	1.15e-12	1.13e-12	4.10e-13	6.12e-13
IMP O2	2.38e-13	3.33e-13	7.61e-14	7.91e-13

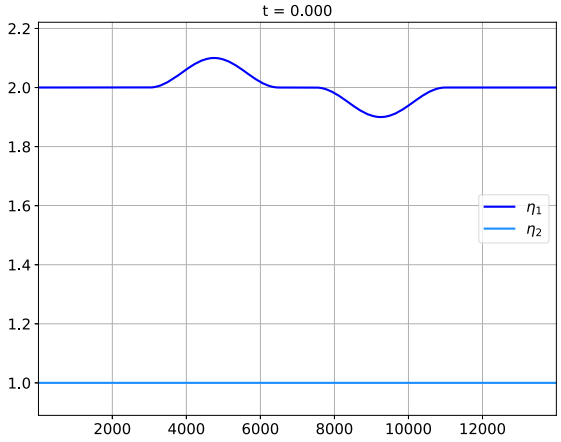

Fig. 7. Initial free surface and interface for the accuracy test.

Table 3
Errors in L^1 norm and convergence rates for the EXP O1 scheme with CFL 0.9.

No. of cells	h_1		q_1		h_2		q_2	
	Error	Order	Error	Order	Error	Order	Error	Order
50	1.30e-02	-	2.07e-03	-	1.43e-02	-	1.01e-01	-
100	6.50e-03	1.00	1.09e-03	0.93	4.07e-03	1.81	5.42e-02	0.90
200	2.90e-03	1.16	4.15e-04	1.39	1.12e-03	1.86	2.08e-02	1.38
400	1.30e-03	1.16	2.01e-04	1.05	3.70e-04	1.60	1.01e-02	1.04
800	6.20e-04	1.07	8.29e-05	1.28	1.26e-04	1.55	4.18e-03	1.28

Table 4
Errors in L^1 norm and convergence rates for the IMP O1 scheme with CFL 1.5.

No. of cells	h_1		q_1		h_2		q_2	
	Error	Order	Error	Order	Error	Order	Error	Order
50	3.00e-02	-	2.98e-02	-	3.37e-02	-	1.51e+00	-
100	1.50e-02	1.00	1.76e-02	0.76	1.94e-02	0.80	8.94e-01	0.76
200	7.00e-03	1.10	9.16e-03	0.94	1.20e-02	0.69	4.65e-01	0.94
400	3.20e-03	1.13	4.41e-03	1.05	6.61e-03	0.86	2.24e-01	1.05
800	1.50e-03	1.09	1.93e-03	1.20	3.11e-03	1.09	9.79e-02	1.20

Table 5
Errors in L^1 norm and convergence rates for the EXP O2 scheme with CFL 0.9.

No. of cells	h_1		q_1		h_2		q_2	
	Error	Order	Error	Order	Error	Order	Error	Order
50	2.24e-03	-	3.72e-04	-	1.10e-02	-	1.85e-02	-
100	5.86e-04	1.94	9.52e-05	1.96	2.85e-03	1.95	4.75e-03	1.96
200	1.47e-04	2.00	2.31e-05	2.05	7.56e-04	1.92	1.15e-03	2.04
400	3.60e-05	2.03	6.26e-06	1.88	2.10e-04	1.85	3.14e-04	1.88
800	7.44e-06	2.27	1.43e-06	2.12	5.18e-05	2.02	7.21e-05	2.12

Table 6
Errors in L^1 norm and convergence rates for the IMP O2 scheme with CFL 1.5.

No. of cells	h_1		q_1		h_2		q_2	
	Error	Order	Error	Order	Error	Order	Error	Order
50	2.16e-03	-	1.61e-02	-	2.24e-02	-	8.18e-01	-
100	5.75e-04	1.91	5.10e-03	1.66	5.58e-03	2.01	2.59e-01	1.66
200	1.44e-04	2.00	1.26e-03	2.02	1.39e-03	2.01	6.41e-02	2.02
400	3.58e-05	2.01	2.86e-04	2.14	3.11e-04	2.16	1.45e-02	2.14
800	8.54e-06	2.07	5.90e-05	2.28	6.80e-05	2.19	2.99e-03	2.28

5.5. Internal shock test case

In order to assess the performance of our numerical schemes in the presence of shock waves, we consider a test case featuring a shock in the interface. The bottom topography is assumed to be flat, and the initial condition within the domain $[0, 10]$ is specified as follows:

$$h_1(x,t=0) = \begin{cases} 0.4, & x < 4, \\ 0.35, & 4 < x < 6, \\ 0.4, & x > 6, \end{cases} \quad h_2(x,t=0) = \begin{cases} 0.2, & x < 4, \\ 0.25, & 4 < x < 6, \\ 0.2, & x > 6, \end{cases}$$

$$q_1(x,t=0) = q_2(x,t=0) = 0.$$

Additionally, we set $r = 0.98$. Note that the free surface η_1 is constant while a shock is present for the variable η_2. The corresponding initial condition is presented in Fig. 8.

Figs. 9, 10, 11, 12 show the numerical solutions obtained at time $t = 1$ for the schemes introduced here, using 200 cells. The results are compared with a reference solution computed using the first-order explicit scheme with 1600 cells. For the explicit schemes, a CFL number of 0.9 has been adopted, whereas for the implicit schemes, we show results for several CFL values equal or larger than 1. The first order implicit scheme allows us to consider bigger CFL values than the second order one without showing big oscillations. This is the reason why we have considered CFL 3 for the first order one and CFL 1.5 for the second order one.

Since this test case involves a shock, larger CFL values for the implicit schemes are not feasible. Recall that the slope limiters are evaluated at time t^n and therefore spurious oscillations appear for very large time steps. For this reason, the second order semi-implicit scheme does not allow the use of big CFL values, since in that case spurious oscillations appear.

With this in mind, we restrict our attention to the first order schemes in order to study the CPU efficiency with respect to the explicit one for large CFL values. In this case, the CPU time needed for the IMP O1 with CFL 3 is 0.27, while the value for the EXP O1 is 0.77, which is almost 3 times faster. As expected, the speed-up increases with the CFL, obtaining 4.5 for CFL 5 and 8.5 for CFL 10.

Moreover, we will also perform additional experiments without shocks where higher CFL values can be used for the second order scheme, thereby allowing for a clearer demonstration of the computational efficiency gains of implicit schemes relative to explicit ones.

Overall, all schemes exhibit satisfactory performance. The second-order explicit scheme introduces some oscillations in the variable η_1, though these oscillations are mitigated when employing implicit schemes, likely due to their inherently more diffusive nature.

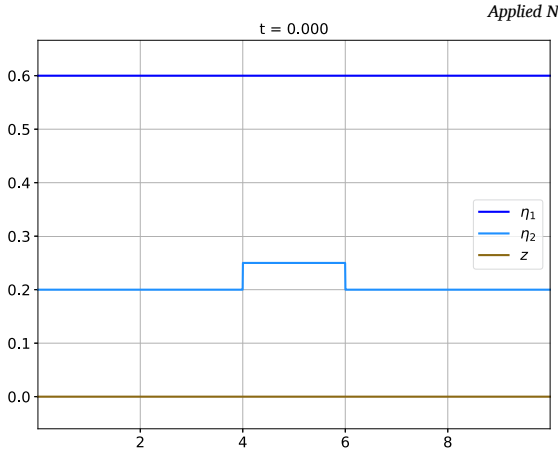

Fig. 8. Initial condition for the internal shock test case.

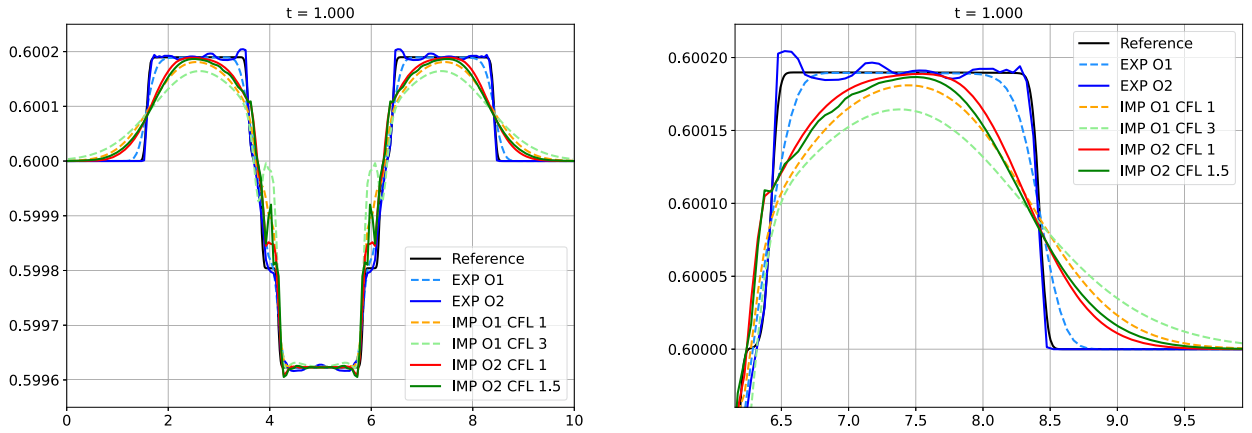

(a) η_1 (b) η_1 (zoom)

Fig. 9. Free surface η_1 and zoom obtained for the internal shock test case at time $t = 1$.

However, the diffusion effect is less pronounced in the second-order implicit scheme compared to the first-order one. Moreover, as the CFL number increases, the diffusive behavior becomes more evident, as expected.

5.6. Tidal wave test

The aim of this test is to assess the gain in computational efficiency of the implicit schemes with respect to the explicit ones. For doing so, we propose a tidal wave test, where we consider a channel with length $L = 14000$, the following bottom topography:

$$z(x) = -\frac{x}{1400} + 40, \tag{24}$$

and a lake-at-rest initial condition given by:

$$h_1(x, t = 0) = 0.4, \quad h_2(x, t = 0) = 0.2 - z(x),$$

$$q_1(x, t = 0) = q_2(x, t = 0) = 0.$$

The value of r is again set to be 0.98 and a tidal wave of amplitude 0.05 is simulated by imposing the following boundary condition for the water heights on the right of the domain:

$$h_1(L, t) = h_1(L, 0) + \varphi_t \alpha_1,$$

$$h_2(L, t) = h_2(L, 0) + \varphi_t \alpha_2.$$

where

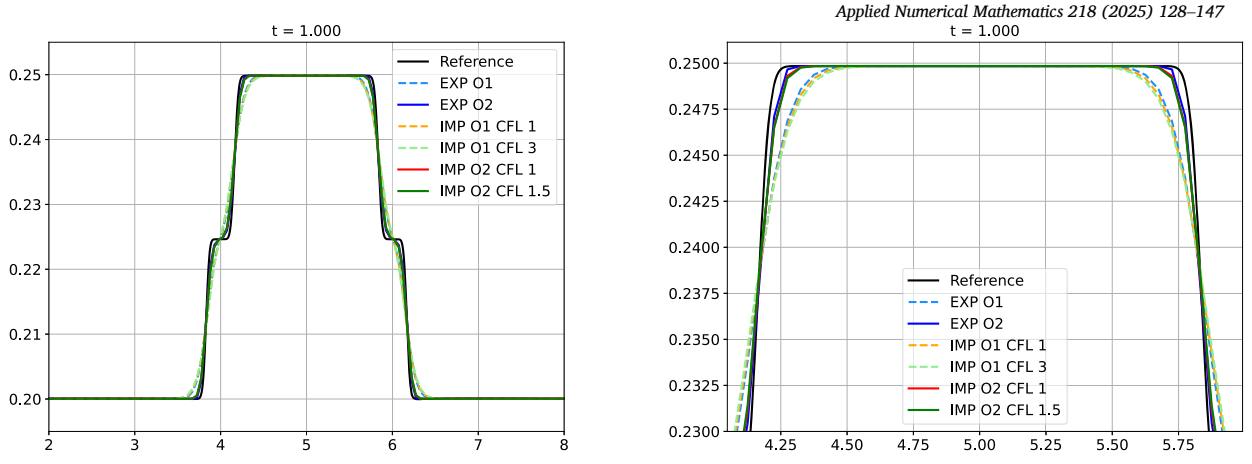

(a) η_2 (b) η_2 (zoom)

Fig. 10. Interface η_2 and zoom obtained for the internal shock test case at time $t = 1$.

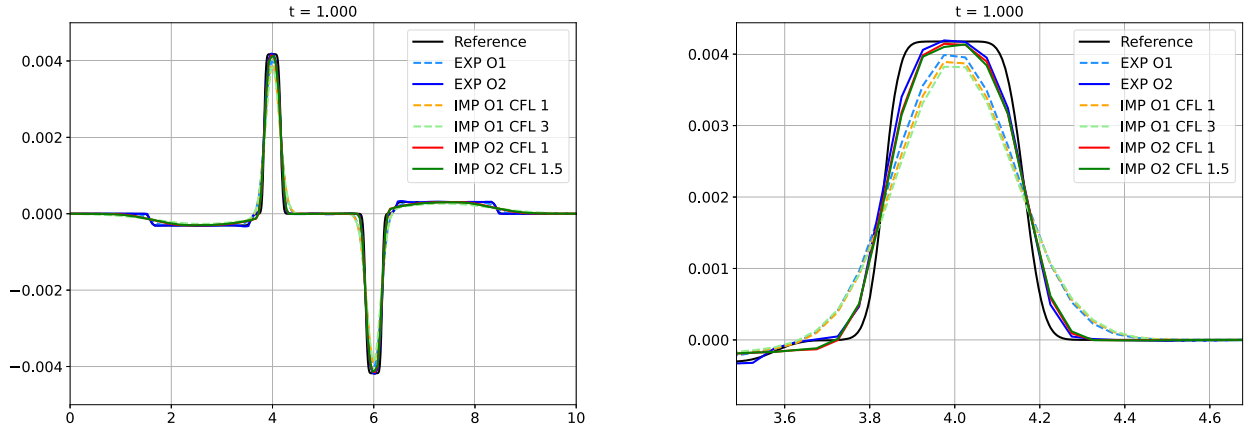

(a) q_1 (b) q_1 (zoom)

Fig. 11. Upper layer discharge q_1 and zoom obtained for the internal shock test case at time $t = 1$.

$$\alpha_i = \frac{h_i(L,0)}{h_1(L,0)+h_2(L,0)} \quad i = 1,2,$$

and

$$\varphi_t = 0.05 \sin\left(\frac{2\pi t}{86400}\right),$$

In this test case, the graphs of the different schemes are almost indistinguishable. In Table 7 we show the CPU time in seconds needed for the different schemes to compute the solution up to time $t = 3600$ using 200 cells. In order to perform this test, we have chosen the maximum CFL for which the solutions do not present oscillations, which in this case is 0.5 for the explicit schemes and 1.5 for the implicit ones. As we can see, the speed-up for the first order schemes is close to 3, while for the second-order ones it is almost 2.

Again, as discussed in the previous test, the first order implicit scheme allows us to consider bigger CFL values than the second order one. Therefore, we have also computed CPU times for this scheme using different CFLs, obtaining the times and speed-ups shown in Table 8. It appears that doubling the CFL number results in a proportional doubling of the speed-up. The graphs for η_1 and q_1 of these simulations are shown in Fig. 13. We can observe that, as expected, when the CFL is increased, the schemes become more diffusive.

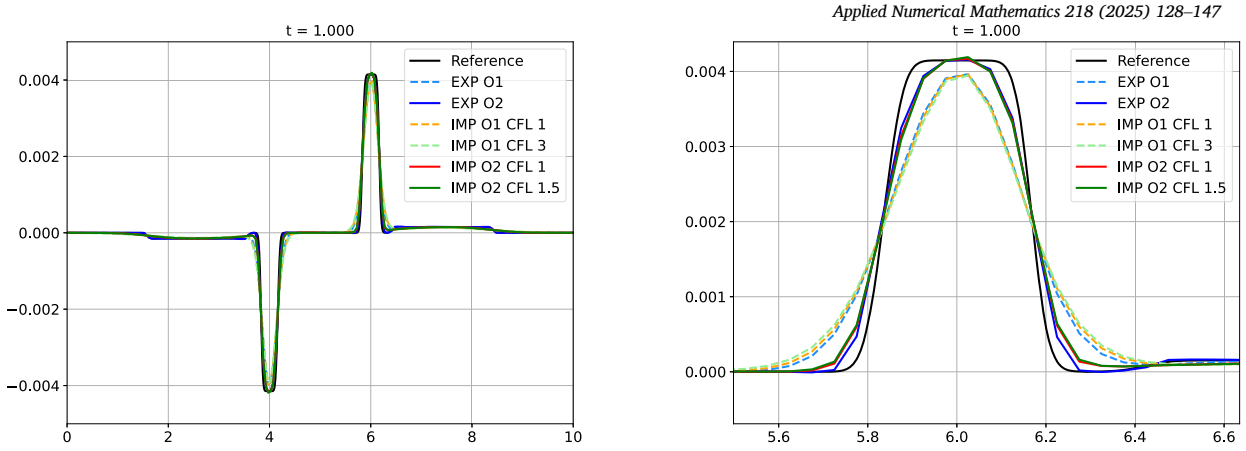

(a) q_2 (b) q_2 (zoom)

Fig. 12. Lower layer discharge q_1 and zoom obtained for the internal shock test case at time $t = 1$.

Table 7
CPU time in seconds needed for the different schemes to compute the tidal wave case solution up to time $t = 3600$ using 200 cells.

	EXP O1	IMP O1	EXP O2	IMP O2
CPU time	128.67	44.55	196.99	107.65

Table 8
CPU time and speed-ups for the first order semi-implicit scheme for different CFL values.

CFL	CPU time	Speed-up
5	13.13	10
10	6.50	20
20	3.37	38
40	1.69	76

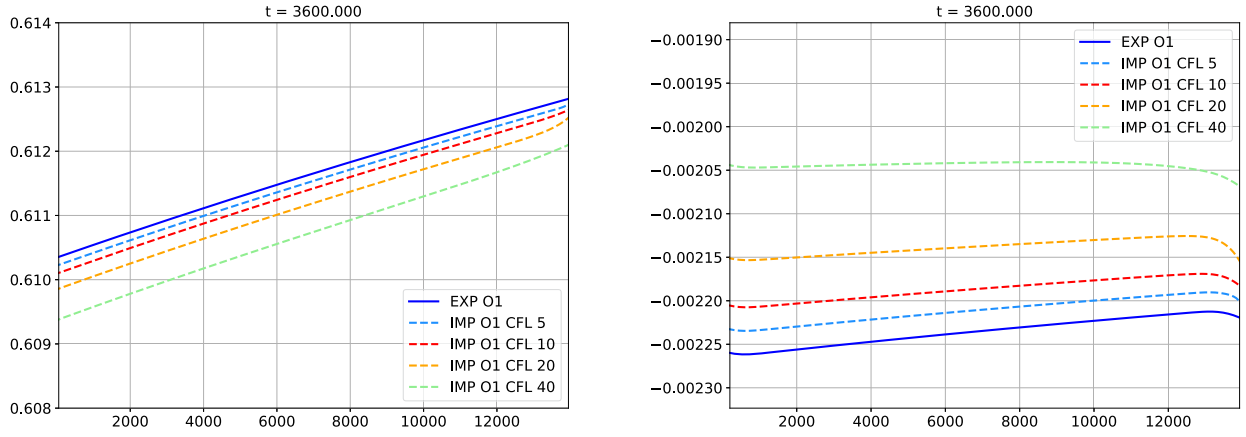

(a) η_1 (b) q_1

Fig. 13. Free surface, η_1, and discharge for the upper layer, q_1, obtained for the tidal wave test case at time $t = 3600$ using different CFL values.

6. Conclusions

In this work, we have developed explicit and semi-implicit numerical schemes for the two-layer shallow water system that exactly preserve every steady state of the problem. To the best of our knowledge, we believe it is the first time that a fully exactly well-balanced scheme is proposed for this system. The methodology proposed here is based on operator splitting and relaxation techniques, and has allowed us to design first- and second-order schemes that maintain both accuracy and stability.

A variety of numerical experiments have been conducted to validate the proposed methods. They include tests to verify the fully exactly well-balanced property, accuracy tests, discontinuous initial conditions involving internal shocks as well as a tidal wave test. In all cases, our schemes exhibit robust behavior and satisfying results.

Eventhough the nonconservative formulation of the acoustic system is used, we have checked that the final numerical scheme preserves the total mass and momentum for the flat topography case.

Particularly noteworthy is the performance of the implicit schemes at high CFL numbers. These schemes remain stable and accurate under large time steps, leading to significant gain in computational efficiency with respect to explicit schemes. For instance, in long-time simulations such as the tidal wave test, the implicit methods yield big speed-ups while preserving the quality of the solution. This makes them especially suitable for situations involving large time scales and low Froude numbers.

CRediT authorship contribution statement

C. Caballero-Cárdenas: Writing – review & editing, Writing – original draft, Visualization, Validation, Supervision, Software, Methodology, Investigation, Formal analysis, Conceptualization. **M.J. Castro:** Writing – review & editing, Writing – original draft, Validation, Supervision, Software, Resources, Project administration, Methodology, Investigation, Funding acquisition, Formal analysis, Conceptualization. **C. Chalons:** Writing – original draft, Supervision, Methodology, Investigation, Formal analysis, Conceptualization. **T. Morales de Luna:** Writing – review & editing, Writing – original draft, Supervision, Software, Methodology, Investigation, Funding acquisition, Formal analysis, Conceptualization. **M.L. Muñoz-Ruiz:** Writing – review & editing, Writing – original draft, Supervision, Methodology, Investigation, Formal analysis, Conceptualization.

Declaration of competing interest

The authors declare that they have no known competing financial interests or personal relationships that could have appeared to influence the work reported in this paper.

Acknowledgements

This work is supported by projects PCI2024-155061-2 and PID2022-137637NB-C21 funded by MCIN/AEI/10.13039/501100011033/ and ERDF A way of making Europe. The authors thank the support of the Centre National de Recherche Scientifique, International Research Project hyPerbolIC models, numerical AnalysiS and Scientific cOmputation (CNRS, IRP PICASSO).

Appendix A. Computation of the stationary solutions

In order to compute the stationary solutions h_1^e and h_2^e given by (3) at any point x_p in a given cell, we use a Newton-based fixed point algorithm. We initialise this fixed point algorithm with the corresponding cell averages, that is, as $h_1^{e,0} = h_1$ and $h_2^{e,0} = h_2$. Then, for each iteration l, we update $h_1^{e,l+1}$ and $h_2^{e,l+1}$ solving the system given by

$$A^l \cdot \Delta h = F^l,$$

where

$$A^l = \begin{pmatrix} 3g\left(h_1^{e,l}\right)^2 + 2\left(g\left(h_2^{e,l} + z(x_p)\right) - C_{2,1}\right) h_1^{e,l} & g\left(h_1^{e,l}\right)^2 \\ rg\left(h_2^{e,l}\right)^2 & 3g(h_2^{e,l})^2 + 2\left(g\left(rh_1^{e,l} + z(x_p)\right) - C_{2,2}\right) h_2^{e,l} \end{pmatrix}$$

and

$$F^l = \begin{pmatrix} g\left(h_1^{e,l}\right)^3 + \left(g\left(h_2^{e,l} + z(x_p)\right) - C_{2,1}\right)\left(h_1^{e,l}\right)^2 + \frac{1}{2}q_1^2 \\ g\left(h_2^l\right)^3 + \left(g\left(rh_1^{e,l} + z(x_p)\right) - C_{2,2}\right)\left(h_2^{e,l}\right)^2 + \frac{1}{2}q_2^2, \end{pmatrix},$$

and finally updating

$$h_1^{l+1} = h_1^l + \Delta h_1,$$
$$h_2^{l+1} = h_2^l + \Delta h_2,$$

where Δh_1 and Δh_2 are the first and second components of the solution of the system Δh.

In the presence of sonic points, the system is not regular. In this case, the technique introduced in [35] could be applied.

References

[1] E. Audusse, F. Bouchut, M.O. Bristeau, R. Klein, B. Perthame, A fast and stable well-balanced scheme with hydrostatic reconstruction for shallow water flows, SIAM J. Sci. Comput. 25 (6) (2004) 2050–2065.
[2] E. Audusse, C. Chalons, P. Ung, A simple well-balanced and positive numerical scheme for the shallow-water system, Commun. Math. Sci. 13 (2015) 1317–1332.
[3] A. Bermúdez, M.E. Vázquez, Upwind methods for hyperbolic conservation laws with source terms, Comput. Fluids 23 (8) (1994) 1049–1071.
[4] C. Berthon, C. Chalons, A fully well-balanced, positive and entropy-satisfying Godunov-type method for the shallow-water equations, Math. Comput. 85 (299) (2015) 1281–1307.
[5] C. Berthon, C. Chalons, S. Cornet, G. Sperone, Fully well-balanced, positive and simple approximate Riemann solver for shallow water equations, Bull. Braz. Math. Soc. 47 (1) (2016) 117–130.
[6] C. Berthon, F. Foucher, Efficient well-balanced hydrostatic upwind schemes for shallow-water equations, J. Comput. Phys. 231 (15) (2012) 4993–5015.
[7] C. Berthon, V. Michel-Dansac, A simple fully well-balanced and entropy preserving scheme for the shallow-water equations, Appl. Math. Lett. 86 (2018) 284–290.
[8] G. Bispen, K.R. Arun, M. Lukáčová-Medvid'ová, S. Noelle, IMEX large time step finite volume methods for low Froude number shallow water flows, Commun. Comput. Phys. 16 (2) (2014) 307–347.
[9] F. Bouchut, Nonlinear Stability of Finite Volume Methods for Hyperbolic Conservation Laws and Well-Balanced Schemes for Sources, Frontiers in Mathematics, Birkhäuser Verlag, Basel, 2004.
[10] F. Bouchut, T. Morales de Luna, A subsonic-well-balanced reconstruction scheme for shallow water flows, SIAM J. Numer. Anal. 48 (5) (2010) 1733–1758.
[11] C. Caballero-Cárdenas, M.J. Castro, C. Chalons, T. Morales de Luna, M.L. Muñoz Ruiz, A semi-implicit fully exactly well-balanced relaxation scheme for the shallow water system, SIAM J. Sci. Comput. 46 (4) (2024) A2503–A2527.
[12] C. Caballero-Cárdenas, M.J. Castro, T. Morales de Luna, M.L. Muñoz-Ruiz, Implicit and implicit-explicit Lagrange-projection finite volume schemes exactly well-balanced for 1D shallow water system, Appl. Math. Comput. 443 (2023) 127784.
[13] C. Caballero-Cárdenas, I. Gómez-Bueno, A. Del Grosso, J. Koellermeier, T. Morales de Luna, A semi-implicit exactly fully well-balanced relaxation scheme for the shallow water linearized moment equations, Comput. Methods Appl. Mech. Eng. 437 (March 2025) 117788.
[14] M.J. Castro, C. Chalons, T. Morales de Luna, A fully well-balanced Lagrange–projection-type scheme for the shallow-water equations, SIAM J. Numer. Anal. 56 (5) (2018) 3071–3098.
[15] M.J. Castro, T. Morales de Luna, C. Parés, Well-balanced schemes and path-conservative numerical methods, in: Rémi Abgrall, Chi-Wang Shu (Eds.), Handbook of Numerical Analysis, in: Handbook of Numerical Methods for Hyperbolic Problems Applied and Modern Issues, vol. 18, Elsevier, 2017, pp. 131–175.
[16] M.J. Castro, E.D. Fernández-Nieto, J. Garres-Díaz, T. Morales de Luna, Discussion on different numerical treatments on the loss of hyperbolicity for the two-layer shallow water system, Adv. Water Resour. 182 (2023) 104587.
[17] M.J. Castro, E.D. Fernández-Nieto, J.M. González-Vida, C. Parés, Numerical treatment of the loss of hyperbolicity of the two-layer shallow water equations, J. Sci. Comput. 48 (2011) 16–40.
[18] M.J. Castro, J.T. Frings, S. Noelle, C. Parés, G. Puppo, On the hyperbolicity of two- and three-luayer shallow water equations, in: Hyperbolic Problems, Series in Contemporary Applied Mathematics, vol. 17, World Scientific, 2012, pp. 337–345.
[19] M.J. Castro, J.A. García-Rodríguez, J.M. González-Vida, J. Macías, C. Parés, Improved FVM for two-layer shallow water models: application to the Strait of Gibraltar, Adv. Eng. Softw. 38 (6) (2007) 386–398.
[20] M.J. Castro, J.A. García-Rodríguez, J.M. González-Vida, J. Macías, C. Parés, M.E. Vázquez-Cendón, Numerical simulation of two-layer shallow water flows through channels with irregular geometry, J. Comput. Phys. 195 (1) (2004) 202–235.
[21] M.J. Castro, A. Kurganov, T. Morales de Luna, Path-conservative central-upwind schemes for nonconservative hyperbolic systems, ESAIM: M2AN 53 (3) (2019) 959–985.
[22] M.J. Castro, J.A. López-García, C. Parés, High order exactly well-balanced numerical methods for shallow water systems, J. Comput. Phys. 246 (2013) 242–264.
[23] M.J. Castro, J. Macías, C. Parés, A Q-scheme for a class of systems of coupled conservation laws with source term. Application to a two-layer 1-D shallow water system, ESAIM: M2AN 35 (1) (2001) 107–127.
[24] M.J. Castro, C. Parés, Well-balanced high-order finite volume methods for systems of balance laws, J. Sci. Comput. 82 (2) (2020).
[25] C. Chalons, M. Girardin, S. Kokh, Large time step and asymptotic preserving numerical schemes for the gas dynamics equations with source terms, SIAM J. Sci. Comput. 35 (6) (2013) A2874–A2902.
[26] C. Chalons, M. Girardin, S. Kokh, Operator-splitting based AP schemes for the 1D and 2D gas dynamics equations with stiff sources, AIMS Ser. Appl. Math. 8 (2014) 607–614.
[27] C. Chalons, M. Girardin, S. Kokh, An all-regime Lagrange-projection like scheme for the gas dynamics equations on unstructured meshes, Commun. Comput. Phys. 20 (1) (2016) 188–233.
[28] C. Chalons, P. Kestener, S. Kokh, M. Stauffert, A large time-step and well-balanced Lagrange-projection type scheme for the shallow water equations, Commun. Math. Sci. 15 (3) (2017) 765–788.
[29] A. Chinnayya, A.-Y. Leroux, N. Seguin, A well-balanced numerical scheme for the approximation of the shallow-water equations with topography: the resonance phenomenon, Int. J. Finite Vol. 1 (2004).
[30] A. del Grosso, M.J. Castro, C. Chalons, T. Morales de Luna, On well-balanced implicit-explicit Lagrange-projection schemes for two-layer shallow water equations, Appl. Math. Comput. 442 (2023) 127702.
[31] E.D. Fernández-Nieto, F. Bouchut, D. Bresch, M.J. Castro, A. Mangeney, A new Savage–Hutter type model for submarine avalanches and generated tsunami, J. Comput. Phys. 227 (16) (2008) 7720–7754.
[32] G. Gallice, Positive and entropy stable Godunov-type schemes for gas dynamics and MHD equations in Lagrangian or Eulerian coordinates, Numer. Math. 94 (4) (2002) 673–713.
[33] G. Gallice, Solveurs simples positifs et entropiques pour les systèmes hyperboliques avec terme source, C. R. Math. 334 (8) (2002) 713–716.
[34] I. Gómez-Bueno, S. Boscarino, M.J. Castro, C. Parés, G. Russo, Implicit and semi-implicit well-balanced finite-volume methods for systems of balance laws, Appl. Numer. Math. 184 (2023) 18–48.
[35] I. Gómez-Bueno, M.J. Castro, C. Parés, Well-Balanced Methods for Compressible Euler Equations with Gravitational Force that Preserve Transonic Stationary Solutions, vol. 35, Springer Science and Business Media Deutschland GmbH, 2024, pp. 85–96.
[36] I. Gómez-Bueno, M.J. Castro, C. Parés, G. Russo, Collocation methods for high-order well-balanced methods for systems of balance laws, Mathematics 9 (15) (2021) 1799.
[37] L. Gosse, A well-balanced flux-vector splitting scheme designed for hyperbolic systems of conservation laws with source terms, Comput. Math. Appl. 39 (9–10) (2000) 135–159.
[38] J.M. Greenberg, A.Y. Leroux, A well-balanced scheme for the numerical processing of source terms in hyperbolic equations, SIAM J. Numer. Anal. 33 (1) (1996) 1–16.

[39] A. Grosso, M.J. Castro, T. Morales de Luna, C. Chalons, On lagrange-projection schemes for shallow water flows over movable bottom with suspended and bedload transport, Numer. Math., Theory Methods Appl. 41 (2023) 10.
[40] J. Kim, R.J. LeVeque, Two-layer shallow water systems and its applications. Hyperbolic Problems: Theory, Numerics and Applications, Proceedings of Symposia in Applied Mathematics, vol. 67.2, American Mathematical Society, 2009, pp. 737–743.
[41] N. Krvavica, M. Tuhtan, G. Jelenić, Analytical implementation of roe solver for two-layer shallow water equations with accurate treatment for loss of hyperbolicity, Adv. Water Resour. 122 (2018) 187–205.
[42] G.I. Marchuk, Metody rasshchepleniya, Nauka, Moskva, 1988.
[43] G.I. Marchuk, Splitting and Alternating Direction Methods, Elsevier, 1990, pp. 197–462.
[44] A. Marquina, S. Serna, Shock-capturing schemes: high accuracy versus total-variation boundedness, PAMM 7 (1) (December 2007) 1024101–1024102.
[45] S. Martínez-Aranda, A. Ramos-Pérez, P. García-Navarro, A 1d shallow-flow model for two-layer flows based on force scheme with wet–dry treatment, J. Hydroinform. 22 (5) (06 2020) 1015–1037.
[46] T. Morales de Luna, M.J. Castro, C. Chalons, High-order fully well-balanced Lagrange-projection scheme for shallow water, Commun. Math. Sci. 18 (3) (2020) 781–807.
[47] J. Murillo, S. Martínez-Aranda, A. Navas-Montilla, P. García-Navarro, Adaptation of flux-based solvers to 2d two-layer shallow flows with variable density including numerical treatment of the loss of hyperbolicity and drying/wetting fronts, J. Hydroinform. 22 (5) (07 2020) 972–1014.
[48] S. Noelle, Y. Xing, C.-W. Shu, High-order well-balanced finite volume WENO schemes for shallow water equation with moving water, J. Comput. Phys. 226 (1) (2007) 29–58.
[49] V.V. Ostapenko, Numerical simulation of wave flows caused by a shoreside landslide, J. Appl. Mech. Tech. Phys. 40 (1999) 647–654.
[50] C. Parés, Numerical methods for nonconservative hyperbolic systems: a theoretical framework, SIAM J. Numer. Anal. 44 (1) (2006) 300–321.
[51] B. Perthame, C. Simeoni, A kinetic scheme for the Saint-Venant system with a source term, Calcolo 38 (2001) 201–231.
[52] B. Ren, C. Parés, High-order weno finite-difference methods for hyperbolic nonconservative systems of partial differential equations, J. Comput. Phys. 535 (2025) 114047.
[53] G. Russo, A. Khe, High order well-balanced schemes based on numerical reconstruction of the equilibrium variables, in: Waves and Stability in Continuous Media, World Scientific, April 2010, pp. 230–241.
[54] L. Sarno, Y. Wang, Y.-C. Tai, R. Martino, A. Carravetta, Asymptotic analysis of the eigenstructure of the two-layer model and a new family of criteria for evaluating the model hyperbolicity, Adv. Water Resour. 154 (2021) 103966.
[55] J.B. Schijf, J.C. Schonfeld, Theoretical considerations on the motion of salt and fresh water, in: Proc. of the Minn. Int. Hydraulics Conv., September 1953, pp. 321–333.
[56] G. Strang, On the construction and comparison of difference schemes, SIAM J. Numer. Anal. 5 (3) (1968) 506–517.
[57] Y. Xing, Exactly well-balanced discontinuous Galerkin methods for the shallow water equations with moving water equilibrium, J. Comput. Phys. 257 (2014) 536–553.
[58] Y. Xing, C.-W. Shu, S. Noelle, On the advantage of well-balanced schemes for moving-water equilibria of the shallow water equations, J. Sci. Comput. 48 (1–3) (2010) 339–349.